



HAL
open science

Improving color correction across camera and illumination changes by contextual sample selection

Hazem Wannous, Yves Lucas, Sylvie Treuillet, Alamin Mansouri, Yvon Voisin

► **To cite this version:**

Hazem Wannous, Yves Lucas, Sylvie Treuillet, Alamin Mansouri, Yvon Voisin. Improving color correction across camera and illumination changes by contextual sample selection. *Journal of Electronic Imaging*, 2012, 21 (2), pp.023015-1–023015-14. 10.1117/1.JEI.21.2.023015 . hal-00719790

HAL Id: hal-00719790

<https://u-bourgogne.hal.science/hal-00719790>

Submitted on 20 Jul 2012

HAL is a multi-disciplinary open access archive for the deposit and dissemination of scientific research documents, whether they are published or not. The documents may come from teaching and research institutions in France or abroad, or from public or private research centers.

L'archive ouverte pluridisciplinaire **HAL**, est destinée au dépôt et à la diffusion de documents scientifiques de niveau recherche, publiés ou non, émanant des établissements d'enseignement et de recherche français ou étrangers, des laboratoires publics ou privés.

Improving color correction across camera and illumination changes by contextual sample selection

Hazem Wannous¹, Yves Lucas², Sylvie Treuillet², Alamin Mansouri³ and Yvon Voisin³

¹ Université de Lille 1, Laboratoire LIFL, Telecom Lille 1, Villeneuve d'Ascq, France.

hazem.wannous@telecom-lille1.eu

² Université d'Orleans, Laboratoire PRISME, IUT de Bourges, Polytech Orleans, France.

yves.lucas@bourges.univ-orleans.fr, sylvie.treuillet@univ-orleans.fr

³ Université de Bourgogne, Laboratoire Le2i, Auxerre France.

alamin.mansouri@u-bourgogne.fr, yvon.voisin@u-bourgogne.fr

Tel: +33 (0) 320 436 427

Abstract

In many tasks of machine vision applications, it is important that recorded colors remain constant, in the real world scene, even under changes of the illuminants and the cameras. Contrary to the human vision system, a machine vision system exhibits inadequate adaptability to the variation of lighting conditions. Automatic white balance control available in commercial cameras is not sufficient to provide reproducible color classification. This paper addresses this problem of color constancy on a large image database acquired with varying digital cameras and lighting conditions. A device-independent color representation may be obtained by applying a chromatic adaptation transform, from a calibrated color checker pattern included in the field of view. Instead of using the standard Macbeth color checker, we suggest selecting judicious colors to design a customized pattern from contextual information. A comparative study demonstrates that this approach ensures a stronger constancy of the colors-of-interest before vision control thus enabling a wide variety of applications.

Index Terms

Color imaging, color checker design, chromatic adaptation.

I. INTRODUCTION

Achieving a perceptually-consistent color representation is a goal of extreme importance for automatic surface inspection problems. But intensity as well as color values displayed by digital cameras do not directly reflect the scene radiance. The color appearance of the surface depends on numerous factors, such as, lighting conditions, viewpoint, material properties and camera adjustment [1]. The radiometric response function of the camera is generally non linear, different for each color channel, and depends on exposure settings such as aperture, focal length and shutter speed. In addition, each commercial digital camera embeds a certain trade-secret color processing such as color demosaicing, white balance adjustment and illumination color correction. Therefore, some precautions have to be taken with commercial digital cameras to insure a consistent color image analysis.

A first approach to color constancy is based on a global calibration process, fixing the conditions of the image acquisition in the laboratory: all images need to be acquired with the same fixed camera under uniform illumination conditions and the same exposure settings. But such an approach is not always possible. Many computer vision applications require color constancy across camera and illumination changes, especially texture mapping on a 3D model [2], [3] or panoramic image mosaicing from multi views [4]. If a scene was recorded by a free handled camera from several view points, there would be color variations between images of the same object. In this case color constancy may be improved by radiometric alignment between images. Some previous works have proposed algorithms for estimating the radiometric response function from differently illuminated images taken with the same camera [5], [6], [7], [2]. In this case, the color textures of images may be aligned by the estimated function. Most of these methods require prior knowledge of exposures on a static scene observed with a fixed camera [5], [6]. Extensions have been proposed, for non static scenes [7] and free movement of the camera [2],

or adding vignetting correction [8]. Such a radiometric alignment addresses images acquired with a sole digital camera but it is not adapted to a large image database acquired over time in different conditions.

For improving color constancy in the context of multiple type of cameras and unconstrained illumination, usual strategy consists in using a calibrated color pattern into the field of view, then, by an optimization process, estimating the best adaptation transform that maps the image color measurements to the corresponding target reference coordinates. This on-line calibration process reduces the color variations due to illumination and camera changes and consequently ensures the reproducibility of the automatic segmentation and classification of the textured color regions on a large image database. We used such a strategy for assessing chronic wounds from color images acquired in several medical centers with different commercial digital cameras [9], [3].

A classical choice for the color pattern is the standard 24-samples Macbeth color checker [10], [11], [12], [13]. This reference pattern covers a very large color space gamut which includes spectral simulations of light and dark skin, blue sky, green foliage, etc. This colormap is well adapted to natural images usually composed of a large number of distinct colors. However, a common drawback of calibration with such a standard pattern is a decrease in performance of constancy when colors of interest are not represented in the color checker. In fact, many surface inspection problems are based on a limited palette of colors. Some works were targeted regarding skin color assessment using a color chart consisting of patches covering the range of skin tones [14], [15]. They investigate the consistency of skin color assessment using several cameras by studying the correlation between the resulting different skin tones extracted from images of the same people and acquired by four different cameras. The target used contains 16 patches covering of the range of human skin, in addition to primary and secondary colors.

Indeed a good strategy for color correction would be to minimize the mean squared error in some judiciously selected areas of the color space, to ensure the constancy of these colors of interest. In our medical context, wound healing diagnosis is based on the examination of the underlying skin tissues. Different types of tissues may be identified by their dominant hue from pink to beefy red, or from yellow

to a brown gradation [9], [3]. But, there is no chance of finding the green or blue patch color in skin tissues and the two skin tones included in the Macbeth chart are not enough to build a wound colormap.

Instead of using the standard Macbeth color checker, we suggest selecting judicious colors from image data base to design a customized pattern before applying usual color correction. The main contribution of this paper is to propose a general methodology to design such a customized color chart using contextual information. This issue deals with the color quantization problem for automatically extracting dominant colors in images by some adaptive clustering algorithms [16], [17], [18], [19]. But our aim was not to classify pixels into their corresponding palette colors, but to design a customized 24-sample color chart. The dominant colors have thus been selected from a set of images instead of a single image. Next, a special sorting algorithm has been developed to reduce these colors to a very small set while saving the best share-out in the color space. A comparative study between correction results obtained with the standard Macbeth color checker chart and our customized one proves that the color distance errors are minimized. The proposed approach ensures a stronger constancy of the color-of-interest and, consequently, provides a more robust automatic classification of skin tissues.

The organization of the paper is as follows: in the next section, we address the color constancy problem in the context of the use of multiple type cameras under unconstrained illumination and present the adopted process for color correction; the proposed methodology for designing a contextual checker chart is detailed in section 3; in section 4, we present the results of the proposed approach and section 5 concludes the paper.

II. COLOR CONSTANCY ACROSS CAMERAS AND ILLUMINATION CHANGES

In its modern formulation, color constancy is the capacity of the human visual system, usually taken as whereby the perceived or apparent color of a surface remains constant despite changes in the intensity and spectral composition of the illumination[20]. This ability, described by the retinex theory, involves both the eye and the brain [21], [22]. But no digital camera has this ability and the color coordinates of pixels are highly dependent on the acquisition conditions (viewpoint, lighting conditions, ...). Color constancy

generally addresses the illumination changes, also called white balancing. But, a second variation is caused by changing the camera. As each digital camera provides a device-dependent RGB color coordinate system and integrates a customized color adjustment processing, a more complete chromatic adaptation transform is required to minimize the color differences between several cameras.

A. Chromatic adaptation transform

One of the specificities of our application is the necessity to collect a large image database over time in multiple medical centers, which involves a constraint related to camera changes. In addition to this constraint, the range of commercial digital cameras is evolving rapidly, with the release of new models every six months. Each digital camera provides a device-dependent RGB color coordinates system and embeds a customized color adjustment processing for white-balancing and demosaicing. Indeed, different cameras can exhibit radically different color responses and can cause significant errors in scene interpretation [12]. Furthermore, digital cameras - even of the same type - do not give mutually consistent outputs. A color calibration step is therefore required to homogenize the photos of the database before the classifier learning stage. Color constancy can be roughly restored by pair-wise correlation for a modeling transfer function based on image color histogram [23]. But the complexity of this approach increases quadratically with the number of cameras and may introduce distortions and quantization errors. In order to ensure color constancy across multiple cameras, we use a calibration process based on the known color target included in the field of view. As each camera has its own RGB color space, the pixel values coming from the camera are defined in an unknown input RGB color space. So, it is necessary to calibrate the acquisition system in order to remove most of the variability introduced by changes in lighting, exposure, and improper white balance. The calibration can be obtained by transforming the pixel values coming from acquired images to other ones defined in a device-independent color space like the standard sRGB color space. This can be achieved by including a small pattern, which contains a limited number of color squares with known colorimetric properties in the image close to the region of interest, in order to deduce or construct a general transform from the RGB to sRGB mapping these patches. One of the

possible methods to determine this mapping is to model it using a polynomial transform, which can be expressed as in Eq. (1):

$$\begin{aligned} \begin{pmatrix} R_c \\ G_c \\ B_c \end{pmatrix} &= \Phi_{RGB \rightarrow sRGB} \begin{pmatrix} R \\ G \\ B \end{pmatrix} \\ &= \begin{pmatrix} a_1 & \cdots & a_m \\ b_1 & \cdots & b_m \\ c_1 & \cdots & c_m \end{pmatrix} \left[\Theta_m \begin{pmatrix} R \\ G \\ B \end{pmatrix} \right] \end{aligned} \quad (1)$$

The transformation Φ is generally based on a polynomial model and the operator Θ_m transforms a 3 element column vector to an m element column vector representing a set of plausible polynomial transforms [24]. Several transforms of varying complexity have been tried, with $m = 3, 6, 8$ and 9 terms respectively (see Table I).

TABLE I
POLYNOMIAL TRANSFORMS OF VARYING COMPLEXITY ORDER.

Order (m)	Transformation (Θ_m)
3	$(R \ G \ B)^t$
6	$(R \ G \ B \ RG \ GB \ BR)^t$
8	$(1 \ R \ G \ B \ RG \ GB \ BR \ RGB)^t$
9	$(R \ G \ B \ RG \ GB \ BR \ R^2 \ G^2 \ B^2)^t$

The coefficients of these transforms a_i , b_i and c_i are determined by the closest match between the reference coordinates of the target patches (already measured with a spectrophotometer) and the coordinates measured by the camera. Each reference color patch provides three equations, allowing us to estimate three by N parameters for N patches. With about twenty color patches, the linear system is over-determined and a least square solution is provided by singular value decomposition. In our context,

the best chromatic adaptation was obtained using the lowest order transformation ($m = 3$) taking into account the inter-channel effects due to the color filter array in front of the CCD sensor. [9], [11]. After acquisition, the calibration procedure computes the RGB to sRGB transformation, and applies it to the whole image.

B. White balancing

A second variation is caused by lighting condition changes. The colorimetric data provided by a digital camera cannot be dissociated from the illuminant spectral distribution. A lot of computer vision algorithms have been developed to model color constancy under illumination changes [25]. Most of them adopt retinex models and the assumption of the independence of each color channel. According to the von Kries chromatic adaptation technique, the human visual system applies a gain to each of the cone cell spectral sensitivity responses so as to keep the adapted appearance of the reference white constant. The white balancing algorithm is an application of von Kries's technique, where coefficient rule rests on the assumption that color constancy is achieved by individually adapting the gains of the three cone responses [26]. Glossy surfaces give rise to specular reflection from light sources. Specular Reflection Assumption presumes that these glossy surfaces have reflectance functions which are constant over a wide range of wavelengths and thus they reflect the actual color of the light source. According to this assumption, to reconstructing the color appearance of an image under white light, we need to scale the image's RGB components to render the specularities white. In the white balancing (white point correction) process, the scale factor for each color channel is just $1/(\text{specular value})$. The white balancing correction model can be represented as follows:

$$\begin{bmatrix} R_c \\ G_c \\ B_c \end{bmatrix} = \begin{bmatrix} RW_{gt}/RW_m & 0 & 0 \\ 0 & GW_{gt}/GW_m & 0 \\ 0 & 0 & BW_{gt}/BW_m \end{bmatrix} \cdot \begin{bmatrix} R \\ G \\ B \end{bmatrix} \quad (2)$$

where $(RW_{gt}, GW_{gt}, BW_{gt})$ are the reference coordinates corresponding to a standard white illuminant, (RW_m, GW_m, BW_m) the measured coordinates and (R_c, G_c, B_c) the corrected ones.

Digital cameras often propose two white balancing modes to correct the color shifts caused by different spectral distributions of the illuminant: automatic or manual. The manual mode requires acquiring an image of a white paper sheet under ambient lighting in order to store white source coordinates, before taking photos. But this is time consuming in the context of a routine visit to a patient's room. The automatic white balance control is based on the stored reference coordinates of a few standard illuminants. Another common hypothesis, referred to as gray world assumption, is made about the general nature of the color components of images. According to this assumption, color balancing algorithms force the images to have a uniform average gray value for its R, G, and B color components in order to remove lighting effects and re-acquire the original colors fairly accurately. The maximal RGB values present in the image are generally considered to represent the illuminating light source. Each pixel color value may then be re-estimated by applying the above ratio matrix. Despite its simple use, this automatic white balance control can not always compensate for the color shift introduced by the ambient lighting.

According to a version of the Retinex algorithm, we suppose that a bright patch available somewhere in the image, reflects the maximum intensity of light possible for each band. Assuming that we are dealing with approximate lambertian reflection, the color coordinates of this patch will be those of the illuminant. However, due to full frame centering, the ambient lighting in the patient's room, composed of several varying sources, may indeed be far from the stored standard illuminants. Therefore, this makes difficult the estimation of the maximum intensity of light possible for each band. When restoring the color appearance of an image, the maximal RGB values in the image may not be localized on a purely white object. For this reason, the calibrated white patch of a checker included in the field of view is required for image color adjustment. The channel ratios applied to the color coordinates of each pixel are based on the white patch coordinates (RW_m, GW_m, BW_m) measured on the checker and the references $(RW_{gt}, GW_{gt}, BW_{gt})$

defined during the calibration stage under D65 standard illuminant [27].

Even if the standard calibration with a target patches as in Macbeth color checker stabilizes the segmentation and classification steps, as illustrated in Fig. 1-b, it can be seen that some interesting colors for medical diagnosis are not optimally corrected. That can be explained by the fact that the minimization of errors is constrained only at some selected points of the color space present on the pattern. A better strategy would be to use a customized checker by selecting judicious colors to insure the closest constancy of these interesting colors. This strategy will be presented in the next section but already we can show improved segmentation result after correction by such a specific pattern (Fig. 1-c).

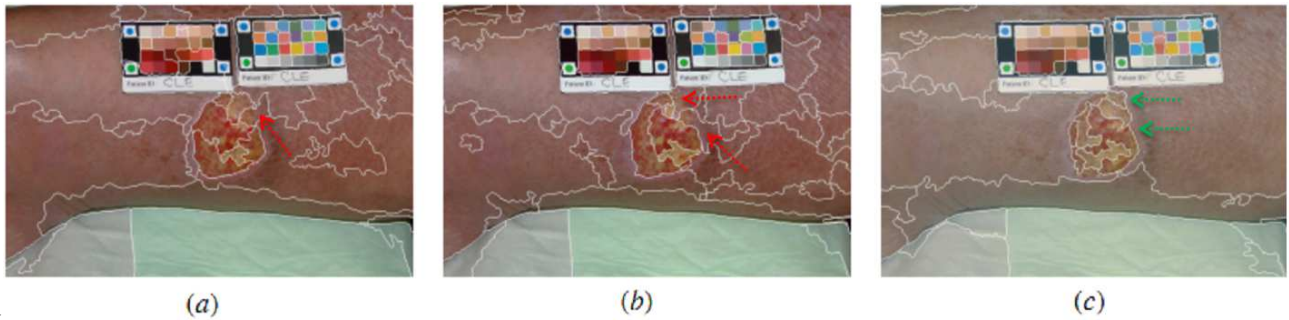


Fig. 1. Segmentation of a wound image acquired under automatic white balance control (a) using only a WB without correction, (b) after correction with standard pattern, (c) after correction with customized pattern.

The segmentation results are improved after correction based on a specific pattern, as it provides a better delineation of tissue samples compared to the medical reference built on clinician tracings [28]. Practically, some regions belonging to two different classes were merged into a single region before and after correction by the Macbeth pattern (red arrow). These regions have been delineated after correction by a specific pattern (green arrow), in addition to the unnecessary over-segmentation of the healthy skin zone in (a) and (b). Note that each segmented region will be classified further into one of four tissue classes (granulation, slough, necrosis and healthy skin), corresponding roughly to red, black, yellow/green and pink shades respectively. so, we should pay much more attention on the segmentation stage as, in our context of a classification driven by un supervised segmentation, any region embedding two different

classes will inevitably lead to a misclassification of a part of this region.

C. Contextual color checker design

The standard Macbeth chart consists of 24 patches chosen to emulate common natural colors such as skin, foliage and sky, in addition to primary colors and a six step grey scale. The colors of this pattern cover an extensive gamut adapted to a large range of images. But, when considering a given surface inspection problem, the vision control generally addresses only a limited palette of colors. Consequently, the color constancy has to be particularly preserved on these colors of interest. In this section, we propose an automatic method to customize the color checker pattern using contextual information. The first thing to do is to collect in live conditions a series of images from the domain of interest, including the standard Macbeth color checker pattern, under varying illuminations and from different cameras. After that, the images are normalized by applying the standard color calibration detailed in the next section. We then compute scene statistics to select judicious colors. To reduce the combinatorial load of the 24-bit color representation, we apply a perceptual color quantization to automatically extract dominant colors from this collection of images. The pre-processing stage includes a peer group filtering algorithm (PGF) to remove impulsive noise from the images and to compute the weighting index used in the later color quantization [29]. Homogeneous neighboring pixels inside the quantization stage are favored by higher weights. Next, the generalized-Lloyd algorithm (GLA) is applied in the perceptive CIELUV space to drastically reduce the number of colors by agglomerative clustering. These choices are justified by the use of a similar pre-processing stage for the JSEG region segmentation adopted here [30], which includes a reliable color quantization stage. Among several advanced segmentation methods, this algorithm proved to be the most efficient on our dermatological image data base. Some details about this comparative study may be found in [9].

The quantization results in a codebook limited to some dominant colors for each image (Fig. 2). Based on this quantization algorithm, a set of 132 colors considered as the most representative for our application were collected from a base of 26 images. This set of colors is obtained by considering only 5 dominant

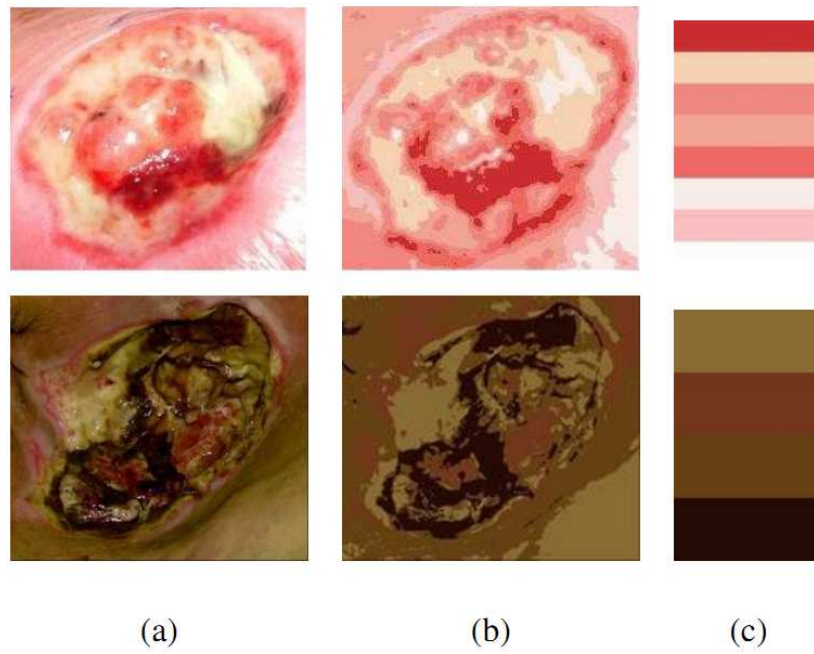


Fig. 2. Color quantization by generalized-Lloyd algorithm (GLA) (a) original image (b) image quantization (c) color codebook.

colors by image added to Black and white color ($5 \times 26 + 2 = 132$). It has been observed that these dominant colors are not uniformly spread in the CIELUV chromaticity plan (u^* , v^*). They form a stretched cloud of points as can be seen on the right side of Fig. 3. A principal component analysis of these data points show that the principal axis is defined by the unit vector $[0.97; 0.24]$. The axis of the largest variance (87% of the total inertia) is highly correlated to the u^* axis, in agreement with the colors of skin tissues which present hue gradation from pink to beefy red, yellow and brown. By comparison, the gamut covered by the Macbeth color checker is really extensive, but only five patches of the Macbeth pattern are confined to the area corresponding to the dominant colors selected by GLA. The next step is to select about twenty judicious colors among the dominant ones in order to design a customized pattern. The proposed selection algorithm implements two basic ideas: give greater importance to the colors with the highest occurrences while preserving the spreading in the chromaticity plan. The iterative process is resumed in the pseudo code (Algorithm 1).

Dividing the set of candidate colors into initial number of cells (L), containing the same number of colors, guarantees an extended recovery of the workspace (samples), while the "If-Else" loop permit to

Require: A set of candidate colors $S_c = \{(L_c, u_c, v_c)^T, c = 1, 2, \dots, N\}$ and the number of representative colors to be selected K

1- Keep all the candidate colors for u and v values in range ∓ 100 in CIELUV space

2- Sort S_c in ordered whole:

- compute the distances ($D = \Delta E_{uv}$) in CIELUV space between all pairs of colors

for a pair of colors i and j : $D = \Delta E_{uv} = \sqrt{(L_{cj} - L_{ci})^2 + (u_{cj} - u_{ci})^2 + (v_{cj} - v_{ci})^2}$

- among $N(N - 1)/2$ pairs of N colors, choose the pair having the smallest distance D

- starting from this pair, sort the colors along the axis of their increasing adjacent distances¹

3- Divide the ordered whole into L ($L < K$) cells containing the same number of colors (n)

4-

for all cells **do**

compute $dsum_c = \sum_{i=1}^{n-1} (D_i)$ for all pairs inside each cell c ;

if $dsum_c \geq$ splitting threshold (τ) **then**

collect the median color in each cell (m color codebook);

else

- merge remaining cells in one

- redivide the later in $K - m$ cells containing the same (new) $dsum_c$

- collect the median color in each cell ($K-m$ color codebook);

end if

end for

Result: K -color codebook $P = \{(L_p, u_p, v_p)^T, p = 1, 2, \dots, K\}$.

¹Choose a color of this pair as the first, the other will be the second, the color having the smallest D with the second one will be the third, and so on.

Algorithm 1: Designing a color checker with a selection of K representative colors.

take into account the distribution of samples (candidate color) in the uniform perceptual space CIELUV. Which satisfies both objectives (1) to cover the color space of the wound image database with a good distribution of it and (2) to be more specific in parts of the color space of higher population. Note that the splitting threshold τ and the initial number L have been tuned empirically in such a way as to obtain a K-color codebook. This sorting algorithm reduces the selected colors to a small set while saving the best share-out in the color space, by balancing the sum of the distance between adjacent colors. The time required to find the origin of the axis in the first step of the algorithm is bounded through the maximum number of about two hundred dominant colors selected by GLA.

This algorithm was applied to a set of 132 candidate colors selected by GLA on the image database, with $K=22$. This choice enabled us to obtain a target with the same patch number as Macbeth and therefore the same shape. The result is illustrated in Fig. 3. Black and white patches are added to the 22 selected colors to complete the customized pattern. The latter has the advantage of proposing a large palette of representative colors included in chronic wound images while maintaining a compact size. Note that, the "For" loop can be performed by iterating the dividing and merging steps n times in the case of large number of candidate colors, which is not necessary for our data.

III. EXPERIMENTAL RESULTS

In this section, we show the effectiveness of the customized pattern based correction with several experiments. We introduce the experimental framework with schematic illustration of the correction process and then present the different experimental tests.

A. *Materials and test protocol*

We use two sets of real images: the first one is composed of images taken under controlled lighting conditions in the laboratory; the second one includes in vivo images taken in the hospital environment. The Macbeth and the customized color charts were printed on a calibrated inkjet color printer using photo paper. The calibration of the overall graphic chain and ICC profiles were generated by PrintFix Pro

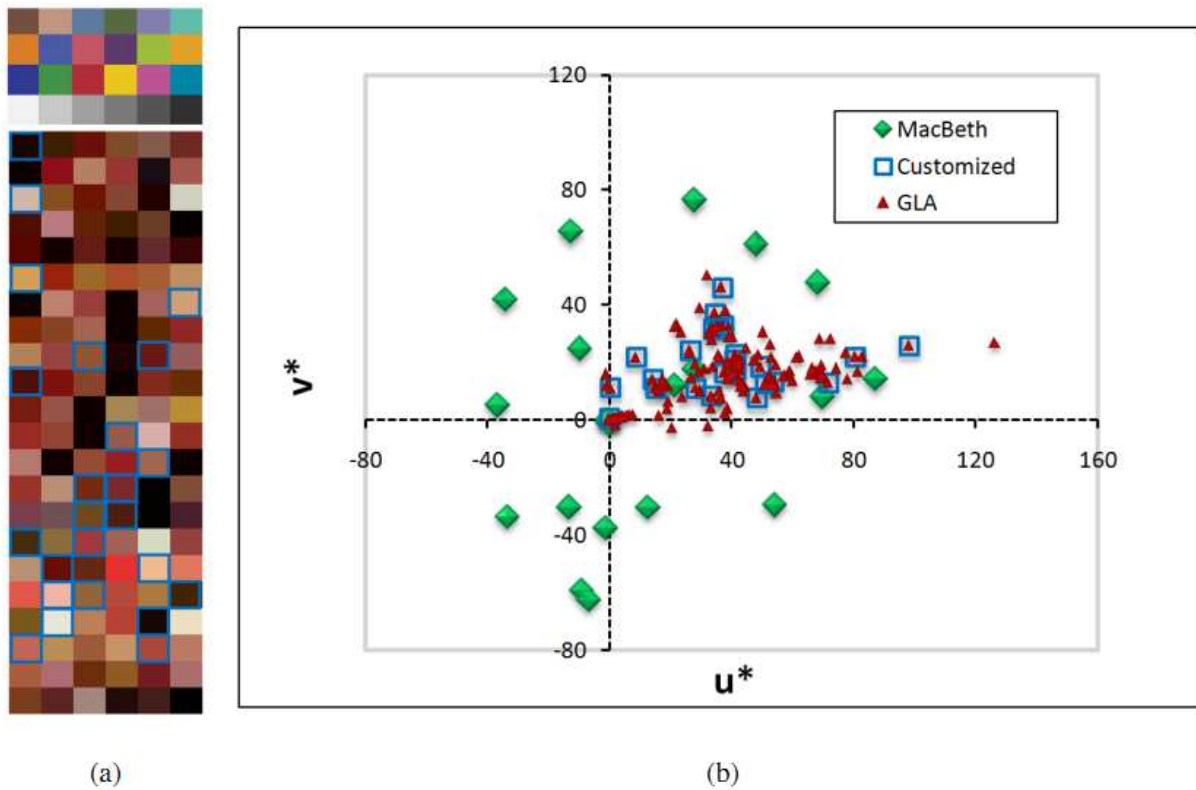


Fig. 3. Selection of specific pattern colors (a) Macbeth pattern and a codebook of 132 colors selected by GLA on the image data base (b) the corresponding patch coordinates in the CIELUV chromaticity plan compared to the Macbeth reference coordinates and the customized color checker coordinates. The 24 patches (22 + Black and white) selected for the Customized pattern are surrounded by a blue square.

software from ColorVision. The printed charts were calibrated with a Minolta CS 1000 spectrophotometer under the standardized D65 illuminant for a 10 degree field of view [27].

In the following tests, the location of the color checker was automatically detected in the images, and the checker was replaced in a facial position by applying a robust homographic transform to remove the perspective effects. Four colored balls placed in the corners of the designed pattern have facilitated automatic detection of the patches. The average RGB coordinates were then extracted in the squared area centered on each patch. The color correction was conveniently computed in sRGB space, but to make a quantitative evaluation, we have adopted the CIELAB perceptually uniform space. The individual inter-sample deviation was computed for each patch by the euclidian distance between the measured coordinates and the reference ones in CIELAB space. Then, we took the average color difference ΔE_{ab} on the 24 patches to estimate globally how different the images are, with respect to the reference image. At each

moment of the correction process, we took into account the CIELAB color distances measured on the 24 patches of Macbeth or the customized target as illustrated in the Fig. 4.

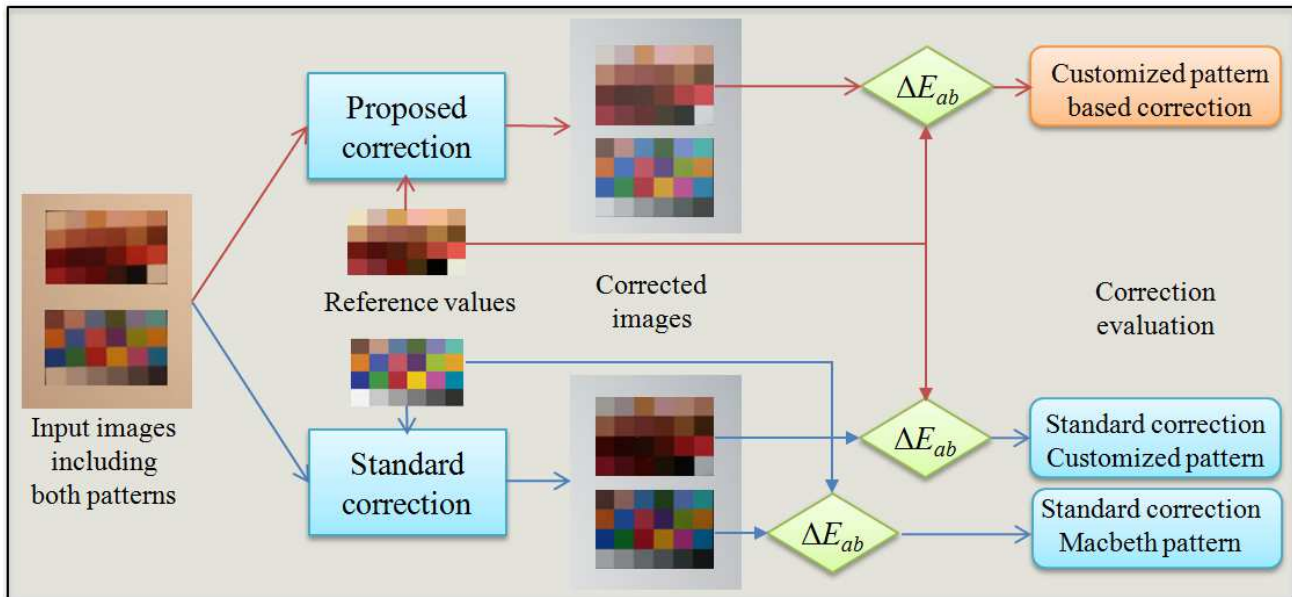


Fig. 4. Experimental protocol for the comparison of standard and customized pattern based correction.

B. Measures under controlled illumination

For comparison purposes, the two color targets (Macbeth and the customized one) were jointly placed under lighting conditions. Images have been captured under different controlled lighting conditions divided into two sets: (1) three lights produced in a light test box: a cool fluorescent light (Illuminant F - 4150 K), an incandescent light (Illuminant A - 2856 K), and daylight-like (Illuminant D65 - 6500 K) (2) four lights produced by commercial lamps: Halogen Eco Classic A OSRAM (H 2900 K), 2 fluorescent (DuluxStar Mini Twist OSRAM F 4000 K and AirPur ELECOLIGHTF 6400 K) and LED LEXMAN (3000-3500 K). Two different types of cameras were tested (a reflex canon EOS 350D and a compact Leica D-Lux 3). The images were stored in raw format to be free from embedded custom color processing. The scene was observed from five different viewpoints: a centering face view and four cardinal views with angles of about 25 degrees, corresponding to our clinical protocol for 3D reconstruction [3], [31]. Each view was captured five times, i.e. a total of 1400 measures to compute the average ΔE_{ab} distance for each camera

and each illuminant, before and after standard and customized pattern based correction. The CIELAB color distances measured on the patches of Macbeth and the customized target are presented in Tables II and III.

TABLE II

CIELAB COLOR DISTANCES MEASURED ON THE 24 PATCHES AFTER CORRECTION WITH THE STANDARD MACBETH COLOR CHECKER AND THE CUSTOMIZED ONE UNDER CONTROLLED ILLUMINATION.

CIELAB distances	illuminant	Canon EOS 350D			Leica D-Lux 3		
		Max	Average	Std	Max	Average	Std
Macbeth target	F	39.78	23.35	4.18	51.13	23.11	1.39
before correction	A	36.17	26.82	2.19	48.78	21.45	1.59
	D65	39.50	28.32	2.21	46.59	24.57	4.44
Customized target	F	31.40	22.82	3.26	21.08	14.28	0.84
before correction	A	32.34	26.21	1.44	23.69	14.12	1.14
	D65	36.80	28.93	1.64	45.21	16.52	4.04
Macbeth target	F	8.45	3.94	0.12	9.89	3.04	0.30
standard correction	A	8.97	4.01	0.13	11.05	3.36	0.41
	D65	7.57	3.88	0.14	7.89	3.26	0.20
Customized target	F	15.67	5.39	0.24	22.41	5.25	0.58
standard correction	A	13.51	5.22	0.29	20.01	5.15	0.54
	D65	12.71	5.24	0.33	17.97	6.05	0.35
Customized target	F	5.87	2.76	0.22	5.40	2.00	0.26
based correction	A	5.46	2.86	0.13	10.15	2.04	0.36
	D65	8.90	2.94	0.17	10.37	1.90	0.23

Before we apply color correction, we can notice very large differences between the two types of digital cameras under different illuminants, with an average of around 25 units. The smaller standard deviation

TABLE III

CIELAB COLOR DISTANCES MEASURED ON THE 24 PATCHES AFTER CORRECTION WITH THE STANDARD MACBETH COLOR CHECKER
AND THE CUSTOMIZED ONE UNDER 4 COMMERCIAL LIGHTS.

CIELAB distances	illuminant	Canon EOS 350D			Leica D-Lux 3		
		Max	Average	Std	Max	Average	Std
Macbeth target before correction	H 2900 K	36.95	33.39	2.04	22.03	18.53	1.53
	F 4000 K	26.15	23.12	1.60	17.20	15.14	1.22
	F 6400 K	23.06	20.55	1.58	20.00	15.20	1.67
	LED 3000 K	33.99	32.51	0.76	24.87	22.67	1.77
Customized target before correction	H 2900 K	36.61	34.09	1.52	23.59	19.95	1.59
	F 4000 K	24.44	22.24	1.22	17.35	15.59	0.77
	F 6400 K	22.55	20.69	1.18	19.14	17.30	0.96
	LED 3000 K	36.73	35.51	0.68	30.73	29.09	1.23
Macbeth target standard correction	H 2900 K	11.00	4.74	0.57	10.49	5.15	0.31
	F 4000 K	9.92	4.51	0.32	8.46	4.26	0.20
	F 4000 K	10.16	4.52	0.24	8.60	4.12	0.26
	LED 3000 K	10.97	3.94	0.30	12.61	4.89	0.32
Customized target standard correction	H 2900 K	14.62	7.38	0.81	22.32	9.14	0.87
	F 4000 K	13.25	6.44	0.54	19.86	8.56	0.68
	F 6400 K	14.13	6.64	0.51	19.79	7.61	0.94
	LED 3000 K	17.05	7.83	0.51	18.51	8.35	0.53
Customized target based correction	H 2900 K	8.19	4.33	0.37	8.42	4.86	0.25
	F 4000 K	6.14	3.62	0.27	7.65	4.02	0.22
	F 6400 K	7.15	3.66	0.27	7.84	4.07	0.36
	LED 3000 K	9.71	4.24	0.26	8.36	4.75	0.27

observed on the customized pattern may be explained by a more restricted range of colors. The correction based on the Macbeth pattern reduces the average ΔE_{ab} on Macbeth color patches by a factor of between 5 to 6, closing the gap to about 3.5-4 for the standard lights produced by test box and about 3.9-5 for the lights produced by commercial lamps. But, for the colors of interest on the customized pattern, the color correction is not acceptable as we can still observe average distances of around 5-6 and maximum values of between 12 to 22. Logically, the color correction is clearly improved with the customized pattern, the bottom error being constrained at around 2-3 for standard lights and 3.6-4.8 for commercial ones) on judicious colors confined to the area of interest in the color space. Note that generally the colors are more affected under the commercial lighting (more than about 10 units). A reason for that may be that, in the digital cameras, the automatic white balancing has been configured to deal with generic lighting sources, rather similar to the standard illuminant provided in our lighting box. On the contrary, the commercial lightings we have tested, recently released on the market due to technological innovations and energy saving product demand, are not very well assigned to one of the classical light sources indexed in the digital camera. This is clearly the case for the LED lamps, which are just entering the consumer market and exhibit very specific spectral responses. The important fact to underline is that ΔE_{ab} is reduced by a similar amount, when dealing with standard illuminants so as with commercial lamps.

A second manipulation is concerned with the influence of the number of patches used during the correction process. The correction is applied by only considering respectively the black and white patches (BW correction), the four color checker generally considered in wound assessment (Black#24-White#19-Yellow#16-Red#15 on the Macbeth checker), and four different subsets of dominant colors. The Macbeth checker, the customized checker and three different subsets of its dominant colors were manually selected for a good recovery of the color Luv space. All correction results obtained for Canon and Leica cameras are given in Table IV and the corresponding patch numbers with the color distances averaged on the 2 cameras (for lights produced in a light test box) are given in Fig. 5.

This test proves that only the BW intensity correction is not sufficient and that more colors have to be

TABLE IV

CIELAB COLOR DISTANCES MEASURED ON THE 24 DOMINANT COLORS OF THE CUSTOMIZED CHECKER AFTER A CORRECTION PROCESS CONSIDERING A VARIABLE NUMBER OF PATCHES.

CIELAB distances	illuminant	Canon EOS 350D			Leica D-Lux 3		
		Max	Average	Std	Max	Average	Std
Before correction	F	31.40	22.82	3.26	21.08	14.28	0.84
	A	32.34	26.21	1.44	23.69	14.12	1.14
	D65	36.80	28.93	1.64	45.21	16.52	4.04
BW correction (2 patches)	F	23.24	18.52	2.00	11.25	8.89	0.97
	A	23.41	21.76	0.79	11.35	8.78	1.19
	D65	22.30	20.83	0.94	11.11	8.98	0.91
BWYR correction (4 patches)	F	6.33	4.31	1.07	7.78	4.83	1.32
	A	5.97	4.43	0.88	9.20	5.05	1.60
	D65	6.15	4.83	0.73	8.59	5.94	1.21
standard correction (Macbeth 24 patches)	F	15.67	5.39	0.24	22.41	5.25	0.58
	A	13.51	5.22	0.29	20.01	5.15	0.54
	D65	12.71	5.24	0.33	17.97	6.05	0.35
Dominant colors correction (4 patches)	F	6.60	3.46	1.17	5.82	2.82	1.18
	A	4.80	3.51	0.62	6.37	2.86	1.35
	D65	5.38	4.30	0.54	6.55	3.01	1.25
Dominant colors correction (6 patches)	F	5.56	3.61	0.80	4.56	2.32	0.87
	A	4.52	3.54	0.46	5.57	2.35	1.13
	D65	4.69	3.85	0.44	5.12	2.56	0.92
Dominant colors correction (12 patches)	F	5.30	3.25	0.90	4.49	2.23	0.88
	A	4.31	3.32	0.52	4.84	2.27	1.03
	D65	4.33	3.54	0.39	4.97	2.51	0.93
Dominant colors correction (24 patches)	F	5.87	2.76	0.22	5.40	2.00	0.26
	A	5.46	2.86	0.13	10.15	2.04	0.36
	D65	8.90	2.94	0.17	10.37	1.90	0.23

TABLE V

CIELAB COLOR DISTANCES MEASURED ON THE 24 DOMINANT COLORS OF THE CUSTOMIZED CHECKER AFTER A CORRECTION PROCESS CONSIDERING A VARIABLE NUMBER OF PATCHES (UNDER COMMERCIAL LIGHTS).

CIELAB distances	illuminant	Canon EOS 350D			Leica D-Lux 3		
		Max	Average	Std	Max	Average	Std
Before correction	H 2900 K	36.61	34.09	1.52	23.59	19.95	1.59
	F 4000 K	24.44	22.24	1.22	17.35	15.59	0.77
	F 6400 K	22.55	20.69	1.18	19.14	17.30	0.96
	LED 3000 K	36.73	35.51	0.68	30.73	29.09	1.23
BW correction (2 patches)	H 2900 K	25.52	23.07	1.33	17.78	15.96	0.95
	F 4000 K	21.67	20.01	0.83	15.82	14.60	0.64
	F 6400 K	19.98	18.86	0.75	16.28	14.83	1.01
	LED 3000 K	25.73	24.62	0.60	25.33	23.65	1.01
BWYR correction (4 patches)	H 2900 K	17.16	8.68	1.13	17.73	10.18	0.90
	F 4000 K	18.00	6.87	0.75	19.92	9.62	0.88
	F 6400 K	18.95	7.46	0.71	18.47	9.23	1.11
	LED 3000 K	15.51	8.76	0.59	15.48	7.61	0.61
standard correction (Macbeth 24 patches)	H 2900 K	18.95	7.38	0.81	19.79	9.14	0.87
	F 4000 K	17.35	6.44	0.54	16.63	8.56	0.68
	F 6400 K	17.63	6.64	0.51	16.57	7.61	0.94
	LED 3000 K	16.77	7.83	0.51	16.17	8.35	0.53
Dominant colors correction (4 patches)	H 2900 K	12.86	6.75	0.65	15.24	8.35	0.42
	F 4000 K	13.17	6.40	0.42	16.22	8.45	0.44
	F 6400 K	13.25	6.54	0.44	17.75	8.28	0.94
	LED 3000 K	13.09	6.43	0.38	16.78	7.94	0.45
Dominant colors correction (6 patches)	H 2900 K	15.11	5.91	0.68	15.15	7.19	0.42
	F 4000 K	10.30	4.57	0.40	14.25	6.63	0.39
	F 6400 K	10.42	4.69	0.44	14.05	5.78	0.58
	LED 3000 K	11.57	5.97	0.31	14.63	7.10	0.30
Dominant colors correction (12 patches)	H 2900 K	10.37	5.25	0.64	11.01	6.36	0.30
	F 4000 K	8.50	3.83	0.34	10.04	5.51	0.31
	F 6400 K	8.53	3.89	0.36	9.91	4.96	0.46
	LED 3000 K	9.42	4.86	0.30	13.47	6.85	0.38
Dominant colors correction (24 patches)	H 2900 K	8.19	4.33	0.47	8.42	4.86	0.25
	F 4000 K	7.14	3.62	0.27	7.65	4.26	0.22
	F 6400 K	7.15	3.66	0.27	7.84	4.07	0.36
	LED 3000 K	7.71	4.24	0.26	9.36	4.89	0.27

considered in the correction process to compensate for the differences between digital cameras. Macbeth target is unsuitable since the limited 4-patch checker BWYR gives better results. Even if correction performance decrease with the number of considered colors, the customized target with four dominant colors already surpasses Macbeth 24-patches checker (see Fig. 5).

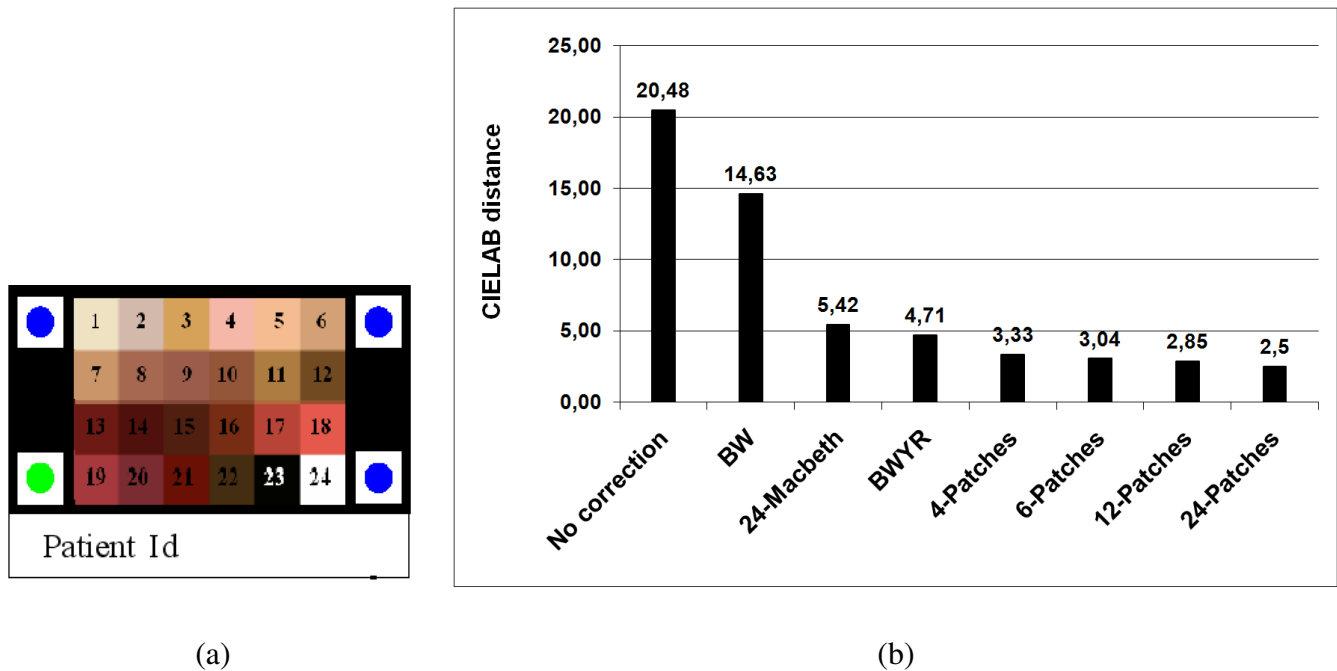


Fig. 5. (a) Customized color checker with blue and green discs at the corners for automatic detection. (b) Averaged CIELAB color distances measured on dominant colors (customized checker) before and after a correction process considering different subsets of patches on the MacBeth checker: BW (only the black #23 and white #24 patches), the complete MacBeth checker (24 patches), Black-White-Yellow-Red patches, and different subsets on the customized one: 4-patches (#7 – 19 – 23 – 24), 6-patches (#3 – 4 – 18 – 20 – 23 – 24), 12-patches (#1 – 3 – 5 – 7 – 8 – 11 – 12 – 17 – 18 – 19 – 23 – 24). The four colored balls at the corners enable automatic pattern detection.

Finally, we measured the influence of the color processing and JPEG compression carried out by the digital camera. These tests were applied on thirty images, taken with the Canon camera and saved in JPEG and RAW format, under the three controlled illuminants. Only the correction by the customized target has been taken into consideration here (see Table VI).

We obtained after correction an averaged CIELAB color distance between 2.68 and 2.76 for JPEG images compared to 1.9 to 2.04 for RAW images, to compare with 16.83 and 21.21 for JPEG images and between 14.12 and 16.51 for RAW images before correction. The JPEG compressed format is more

TABLE VI

CIELAB COLOR DISTANCES MEASURED ON THE 24 PATCHES OF THE CUSTOMIZED COLOR CHECKER, IN JPEG AND RAW FORMAT.

CIELAB distances	illuminant	JPEG format			RAW format		
		Max	Average	Std	Max	Average	Std
before correction	Cool	25.32	16.83	1.57	21.08	14.28	1.84
	A	23.98	17.93	1.00	23.69	14.12	1.14
	D65	41.99	21.21	3.18	45.21	16.51	4.09
correction with customized target	Cool	6.95	2.68	0.34	5.40	2.00	0.26
	A	7.19	2.73	0.44	10.15	2.04	0.36
	D65	7.99	2.76	0.30	10.37	1.90	0.23

convenient for storing a large image database, but it implies no control on embedded color processing, such as demosaicing or white balancing which are specific to each camera type. However, the tests prove that the performance of the correction is not significantly degraded by all these transformations.

C. Influence of the color pattern exposure conditions

Placing a color pattern in the field view obviously improves the color correction process, but one should not forget that the pattern itself is not the main element of the scene. We mean that it will not always be optimally exposed during the image capture, as the exposure time is generally computed on the center of the image, where lies the object of interest. Consequently, it is advisable to examine the influence of the pattern exposure level on the performance of the color correction. Under exposure and also over exposure have important effects on the spectral response, leading typically to washed out shades.

To evaluate the effect of color alteration due to an incorrect exposition, we used the exposure compensation setting available on digital cameras, commonly referred to as exposition value (EV). An exposure compensation of $+1EV$ (or $+1$ step) means to increase exposure by using either a double exposure time or a f-number divided by the root of 2. So, the sense of exposure compensation is opposite that of the classical EV scale itself, which indicates the photometric quantity of luminous exposure rather

than combinations of camera settings. Practically, we exposed the Macbeth and customized pattern with a series of exposure compensations from $-2EV$ to $+2EV$ with $1/3EV$ steps under the full spectrum fluorescent commercial lighting (6400 K).

Although all camera settings with the same exposure value, obtained with different combinations of shutter speed and aperture, nominally give the same exposure, they do not necessarily give the same picture. At a first glance, we can answer that the shutter speed determines the amount of motion blur and the aperture determines the depth of field. In fact, we are more concerned here with other effects: firstly, the image sensor may exhibit reciprocity failure, which is a change of light sensitivity dependent on the intensity, and secondly, the signal to noise ratio will be dependent of the exposure time, as photon shot noise, so as dark noise and read noise have increased effects on low intensity conditions which lead to long exposure time and low signal to noise ratios. So, to examine the impact of camera noise on the color correction process, we have completed the preceding bracketing test with a series of 9 shutter speed/aperture combinations, from $f/2.8$ to $f/11$ f-numbers, with one-third-stops (the corresponding shutter speeds are automatically set by the digital camera in the aperture priority exposure mode).

As a result, we can plot the variations of ΔE_{ab} as a function of the exposition value and the f-number. It is convenient and concise to display these variations on the same graph, starting with data obtained with $-2EV$ exposure compensation for the 9 aperture f-numbers and continuing toward the $+2EV$ compensation (Fig. 6).

Several observations can be made on the results:

- before color correction, ΔE_{ab} is highly dependent of the exposure compensation applied, especially for under-exposed pictures ($EV < 0$), with a minimum shifted by one from the nominal exposure ($EV = 0$). The influence of exposure time, clearly visible on the graph, is expressed by the pseudo-periodic structure of the graph, as for each compensation value we plot successively the data obtained for each aperture. We can note that each digital camera produces a different and typical signature when the f-number is increased, with larger changes for the Canon EOS 350D than for the Leica

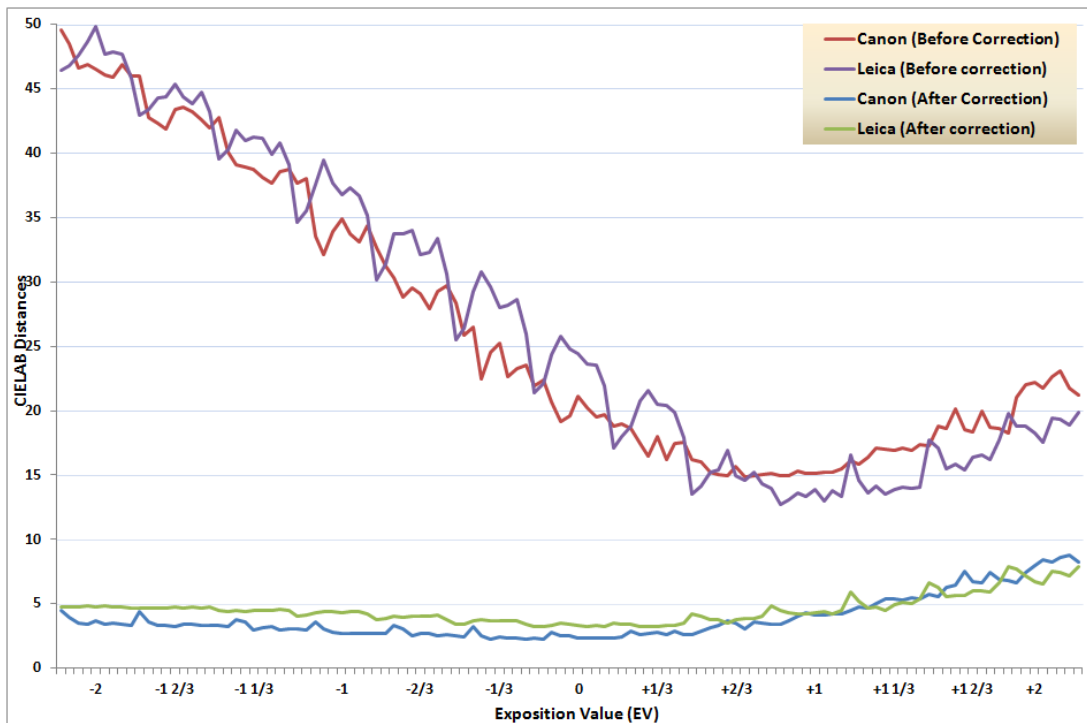


Fig. 6. The variations of ΔE_{ab} as a function of the exposition value and the f-number (from $f/2.8$ to $f/11$).

D-Lux 3.

- after color correction, the most important fact is that ΔE_{ab} is strongly reduced and that it is neither affected by under exposure nor aperture selection. For $EV > 1$, ΔE_{ab} is increasing but slowly, meaning that over exposition is more difficult to manage than under exposition. To resume, we can conclude that, globally, the exposure conditions do not influence at all the performance of the color correction, so long as the pattern is not over exposed beyond $+1EV$. As the pattern is typically placed on the side of the field of view, this last situation is less likely to occur.

D. In vivo images

To evaluate the customized pattern based correction in real conditions, the same tests were applied to a collection of in vivo images taken during patient examination in several hospitals (see Fig. 8). We note that results are always averaged on the 24 patches of the standard Macbeth color checker and the customized one.

For the last 8 real JPEG images presented in Fig. 8, we obtained an averaged CIELAB color distance



Fig. 7. Collection of in vivo images.

of 3.37 ∓ 0.47 by customized pattern based correction compared to 10.68 ∓ 1.74 by Customized standard correction (see Table VII). This confirms that the contextual color correction using the customized pattern results is a higher degree of constancy for the colors of interest.

TABLE VII

CIELAB COLOR DISTANCES MEASURED ON THE 24 PATCHES OF THE STANDARD MACBETH COLOR CHECKER AND THE CUSTOMIZED ONE DESIGNED FOR IN VIVO IMAGES.

CIELAB distances	in vivo images (JPEG)		
	Max	Average	Std
Macbeth before correction	29.28	15.07	6.56
customized before correction	34.82	20.02	4.05
Macbeth standard correction	9.74	4.24	0.25
customized standard correction	27.88	10.68	1.74
customized pattern based correction	8.47	3.37	0.47

The benefits of the customized color correction may also be verified on the color descriptors of the tissue samples. The Mean Color Descriptor (MCD) in the CIELAB space, which is used as feature in the tissue classification step [28], has been estimated for several hundreds regions extracted by automatic segmentation of the corrected images (Fig. 9). The $L^*a^*b^*$ values of the MCD of each region are represented in the chromaticity plan before and after correction (see Fig. ??). For each of the three classes of tissue,

the customized pattern based correction produces a shift in the dominant colors and draws the samples closer : a drastically constricted cloud means that the color descriptors are more stable. Conversely, the standard correction with Macbeth checker is unsuitable for images composed out of a limited palette of colors.

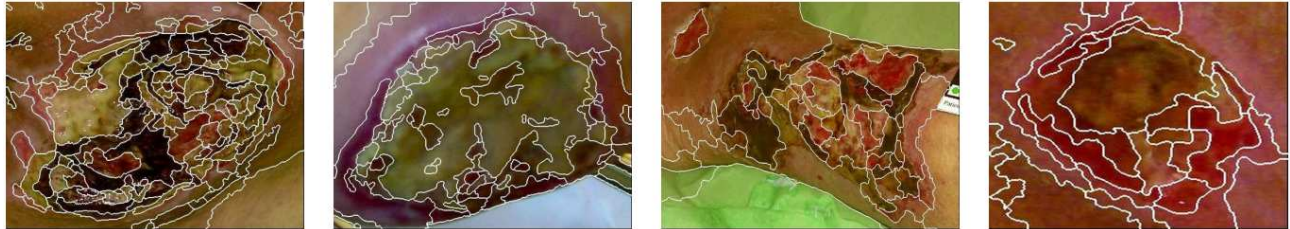


Fig. 8. Examples of segmented regions.

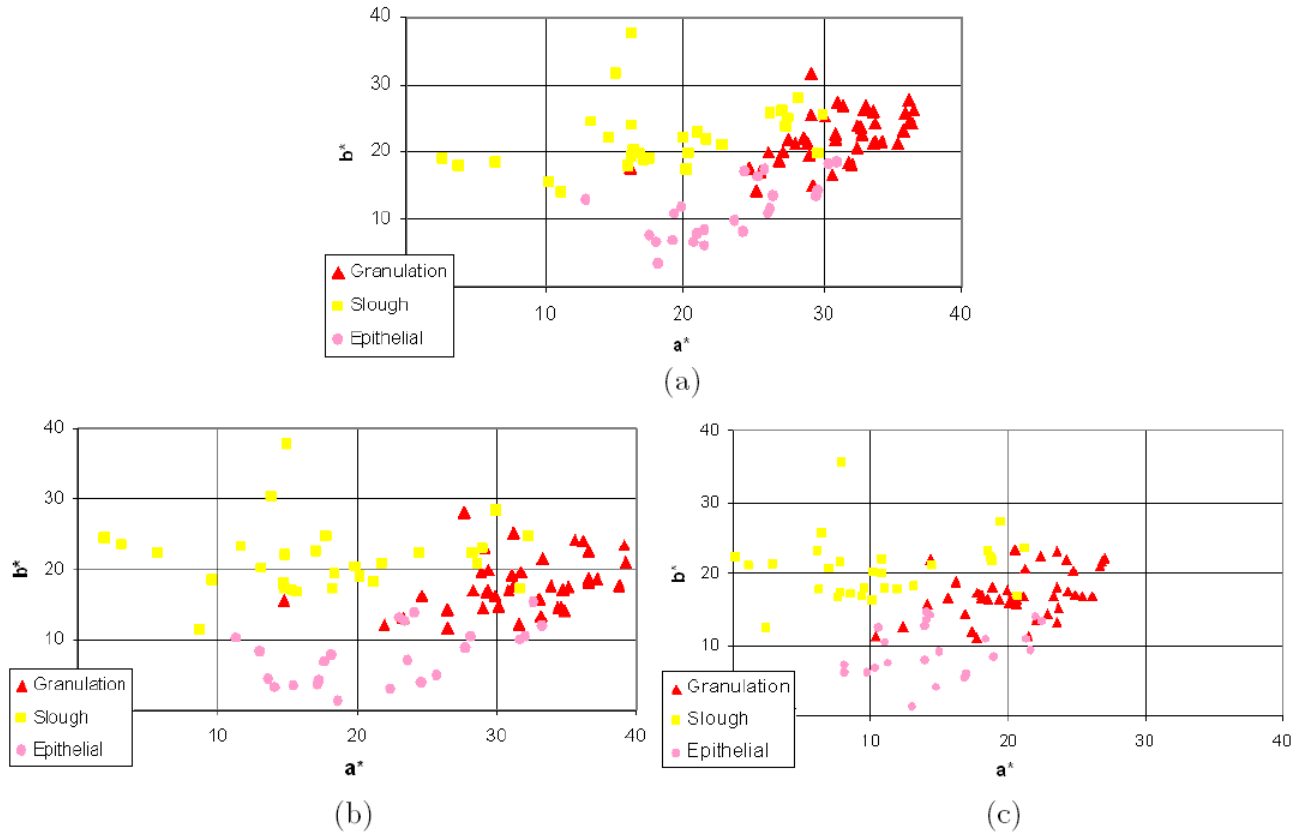


Fig. 9. $L^*a^*b^*$ values of the color descriptor (MCD) of each region represented in the chromaticity plan before and after correction with Macbeth and customized checker. (a) without correction (b) standard correction with Macbeth checker (c) customized pattern based correction with customized checker.

Finally, to assess the practical impact of the color correction step at the output of the image processing

chain, we have compared the performance of skin tissue classification including or not color correction. The performance of the classification of the skin tissues is improved and a better agreement is obtained with the medical expert. We obtained an averaged performance of 67% before and 83% after correction when including the correction step [28]. The performances of tissue classification are given in Table VIII.

TABLE VIII

THE PERFORMANCE OF TISSUE CLASSIFICATION BEFORE AND AFTER COLOR CORRECTION.

<i>Tissue class</i>	<i>No correction</i>	<i>Correction</i>
<i>Granulation</i>	0.85	0.85
<i>Slough</i>	0.52	0.70
<i>necrosis</i>	0.50	0.83
<i>Health skin</i>	0.84	0.92
<i>Average</i>	0.67	0.83

IV. CONCLUSION

This paper deals with color constancy on a large image database acquired with varying digital cameras and lighting conditions. Automatic white balance control available on commercial cameras is not sufficient to provide reproducible surface inspection or classification results. The instability in color rendering may be significantly reduced by applying a color calibration step with a color checker pattern included in the field of view. A device-independent color representation may then be obtained by applying a chromatic adaptation transform, without the necessity of re-calibrating the cameras when the lighting conditions change. Instead of using the standard Macbeth color checker, we suggest selecting adapted colors to design a customized chart using contextual information. A comparative study demonstrates that this approach ensures the closest constancy of the colors of interest for vision inspection tasks. We conclude that using heterogeneous cameras and varying ambient illumination in the patient's room is possible for computer aided diagnosis of skin lesions. While designed for optimum color constancy in cutaneous imaging, the proposed approach for color checker customization can be applied to many surface inspection problems

requiring a limited palette of colors. These experiments prove that it is possible to customize and produce a low cost color checker pattern surpassing the standard Macbeth checker for improved color constancy across illumination and camera changes. Future works will be centered on the optimization of the selection of the dominant colors by systematically taking into account color frequency in the image data base and by investigating color histogram support for minimizing weighted color distances. Finally, as we have developed new tools for 3D scene reconstruction from images taken from different view points, we intend to combine several color pattern images to improve again color correction.

ACKNOWLEDGMENT

This research program is supported by the European Social Funds and by the French Delegation of Research and Technology.

REFERENCES

- [1] K. Barnard and B. Funt, "Camera characterization for color research," *Color Research and Application*, vol. 27(3), pp. 153–164, 2002.
- [2] S. Kim and M. Pollefeys, "Radiometric self-alignment of image sequences," in *Int. Conf. on Computer Vision and Pattern Recognition*, vol. 1, 2004, pp. 645–651.
- [3] H. Wannous, Y. Lucas, and S. Treuillet, "Enhanced assessment of the wound-healing process by accurate multiview tissue classification," *IEEE Trans. on Med. Imag.*, vol. 30, no. 2, pp. 315–326, 2011.
- [4] R. Szeliski and H. Shum, "Creating full view panoramic image mosaics and environment map," in *Annual Conf. on Computer Graphics*, 1997, p. 251258.
- [5] P. E. Debevec and M. Jitendra, "Recovering high dynamic range radiance maps from photographs," in *Proc. of the 24th annual conference on Computer graphics and interactive techniques*, 1997, pp. 369–378.
- [6] T. Mitsunaga and S. Nayar, "Radiometric self-calibration," in *Conf. on Vision and Pattern Recognition*, vol. 2,, 1999, pp. 374–380.
- [7] M. Grossberg and S. Nayar, "What can be known about the radiometric response function from images ?" in *Lecture Notes in Computer Science (ECCV)*, vol. 2353, 2002, pp. 393–413.
- [8] S. Kim and M. Pollefeys, "Robust radiometric calibration and vignetting correction," *IEEE Trans. on Pattern Analysis and Mach. Intell.*, vol. 30 (4), pp. 562–576, 2008.
- [9] H. Wannous, S. Treuillet, and Y. Lucas, "Supervised tissue classification from color images for a complete wound assessment tool," in *29th Inter. Conf. of the IEEE Eng. in Med. and Bio. Soc. EMBS'07*, 2007, pp. 6031–6034.

- [10] K. Barnard, L. Martin, A. Coath, and B. Funt, "A comparison of computational colour constancy algorithms, part ii : Experiments with image data," *IEEE Trans. on Image Processing*, vol. 11(9), pp. 985–999, 2002.
- [11] Y. V. Haeghen, J. M. Naeyaert, I. Lemahieu, and W. Philips, "An imaging system with calibrated color image acquisition for use in dermatology." *IEEE Trans. on Medical Imaging*, vol. 19, no. 7, pp. 722–730, July 2000.
- [12] A. Ilie and G. Welch, "Ensuring color consistency across multiple cameras," in *IEEE Int. Conf. on Computer Vision*, vol. 2, 2005, pp. 1268–1275.
- [13] A. Mansouri, F. Marzani, and P. Gouton, "Development of a protocol for ccd calibration: application to a multispectral imaging system," *IJRA*, vol. 20(2), pp. pp. 94–100, 2005.
- [14] M. Harville, H. Baker, N. Bhatti, and S. Susstrunk, "Consistent image-based measurement and classification of skin color," in *Proc. of IEEE Int. Conf. on Image Process*, vol. 2, 2005, pp. 374–377.
- [15] J. Marguier, N. Bhatti, H. Baker, M. Harville, and S. Ssstrunk, "Assessing human skin color from uncalibrated images." *International Journal of Imaging Systems and Technology*, vol. 17, pp. 143–151, 2007.
- [16] I.-S. Hsieh and K.-C. Fan, "An adaptive clustering algorithm for color quantization," *Pattern Recognition Letters*, vol. 21(4), pp. 337–346, 2000.
- [17] S. Cheng and C. Yang, "A fast and novel technique for color quantization using reduction of color space dimensionality," *Pattern Recognition Letters*, vol. 22 (8), pp. 845–856, 2001.
- [18] Y. Sirisathitkul, S. Auwatanamongkol, and B. Uyyanonvara, "Color image quantization using distances between adjacent colors along the color axis with highest color variance," *Pattern Recognition Letters*, vol. 25(9), pp. 1025–1043, 2004.
- [19] B. A. et al., "Perceptual color clustering for image segmentation based on ciede 2000 color distance," in *11th Congress of the International Colour Association (AIC) 2009*, 2009.
- [20] D. Foster, "Color constancy," *Vision Research*, vol. 51, pp. 674–700.
- [21] E. Land and J. McCann, "Lightness and retinex theory." *Journal of Optical Society of America*, vol. 61, pp. 1–11, 1971.
- [22] E. H. Land, "The retinex theory of color vision," *Scientific American*, pp. 108–128, 1977.
- [23] F. Porikli, "Inter-camera color calibration by cross-correlation model function," in *IEEE Int. Conf. on Image Proc*, vol. 2, 2003, pp. 133–136.
- [24] H. Kang, "Color technology for electronic imaging devices." in *SPIE Optical Engineering Press*, 1997.
- [25] J. McCann, "Mechanism of color constancy," in *IS&T/SID Conf. on Color Imaging*, vol. 12, 2004, pp. 29–36.
- [26] M. Ebner, *Color constancy*. John Wiley and Sons, 19 juin 2007.
- [27] CIE, "Colorimetry part 2: Standard illuminants for colorimetry," Joint ISO/CIE Standard ISO 11664-2:2008(E)/CIE S 014-2/E:2006, CIE Central Bureau, Kegelgasse 27, A-1030 Vienna, Austria, Tech. Rep., 2008.
- [28] H. Wannous, S. Treuillet, and Y. Lucas, "Robust tissue classification for reproducible wound assessment in telemedicine environments," *J. Electronic Imaging*, vol. 19(2), p. 023002, 2010.

- [29] Y. Deng, S. Kenney, M. Moore, and B. S. Manjunath, "Peer group filtering and perceptual color image quantization," in *IEEE Inter. Symp. on Circ. and Sys. VLSI (ISCAS'99)*, vol. 4, Orlando, FL, June 1999, pp. 21–24.
- [30] Y. Deng and B. S. Manjunath, "Unsupervised segmentation of colour-texture regions in images and video," *IEEE Trans. on Pattern Analysis and Machine Intelligence (PAMI '01)*, vol. 23, pp. 800–810, 2001.
- [31] S. Treuillet, B. Albouy, and Y. Lucas, "Three-dimensional assessment of skin wounds using a standard digital camera," *IEEE Trans. on Med. Imag.*, vol. 28, pp. 752–762, May 2009.